HEFAT2014
10th International Conference on Heat Transfer, Fluid Mechanics and Thermodynamics
14 – 16 July 2014
Orlando, Florida

THERMAL AND THERMODYNAMIC ANALYSIS OF A PARABOLIC TROUGH RECEIVER AT DIFFERENT CONCENTRATION RATIOS AND RIM ANGLES

Mwesigye A.[1,2], Le Roux, W.G.[1], Bello-Ochende T.[3,*] and Meyer J.P.[1]
*Author for correspondence
[1]Department of Mechanical and Aeronautical Engineering,
University of Pretoria, Pretoria, 0002, South Africa,
[2]Department of Mechanical Engineering, Tshwane University of Technology,
Private Bag X 680, Pretoria, 0001, South Africa,
[3]Department of Mechanical Engineering, University of Cape Town,
Private Bag X3, Rondebosch 7701, South Africa,
E-mail: tunde.bello-ochende@uct.ac.za

ABSTRACT

In this paper, a three dimensional analysis of the thermal and thermodynamic performance of a parabolic trough receiver is investigated. The analysis involves determination of the heat flux on the receiver's absorber tube using the Monte Carlo ray-trace method and using computational fluid dynamics to investigate the thermal and thermodynamic performance. Our analysis shows that the use of higher concentration ratios increases the receiver's temperature gradients and entropy generation rates. For rim angles lower than 60°, the high heat flux peaks result in high temperature gradients in the receiver's absorber tube as well as high entropy generation rates. The absorber tube temperature gradients and entropy generation rates do not change significantly as rim angles increase above 80°. The influence of rim angles on receiver thermal performance reduces as the flow rates increase above 8.55×10^{-3} m^3/s at all inlet temperatures for any given concentration ratio.

INTRODUCTION

The increasing need to minimise the environmental impacts of energy generation, need to meet the ever-increasing energy demand and the need to ensure security of energy supply have increased exploitation and use of renewable energy resources considerably. Solar energy is one of the renewable energy resources and has received considerable attention in the recent past. Solar energy has potential to supply a significant portion of the world's energy demand [1].

The parabolic trough technology is the most commercially and technically developed of the concentrated solar power technologies available today. The parabolic trough systems consist of a mirror bent into a parabolic shape, a linear receiver at the collector's focus and supporting structures. The linear receiver of the parabolic trough is a crucial part of the entire system; its performance greatly affects the performance of the entire collector system. The receiver consists of an absorber tube enclosed in a glass envelope. The absorber tube is selectively coated to increase absorption of solar radiation and reduce emission of infrared radiation. The space between the glass envelope and the absorber tube is evacuated to suppress the convection heat loss in the annulus space.

NOMENCLATURE

a	[m]	Collector aperture width
A_a	[m^2]	Projected aperture area
A_r	[m^2]	Projected absorber tube area
Be	[-]	Bejan number
C_R	[-]	Concentration ratio = A_a/A_r
d_c	[m]	Spacing between absorber tube and glass cover
DNI	[W/m^2]	Direct normal irradiance
d_{gi}	[m]	Glass cover internal diameter
d_{go}	[m]	Glass cover outer diameter
d_{ri}	[m]	Absorber tube inner diameter
d_{ro}	[m]	Absorber tube outer diameter
f	[m]	Collector focal length
g	[m/s^2]	Acceleration due to gravity
h	[W/m^2 K]	Convective heat transfer coefficient
k	[W/mK]	Thermal conductivity
L	[L]	Length
LCR	[-]	Local concentration ratio
P	[Pa]	Pressure
Pr	[-]	Prandtl number
Q_{loss}	[W]	Receiver thermal loss
Ra	[-]	Rayleigh number
Re	[-]	Reynolds number
S'_{gen}	[W/m]	Entropy generation rate per unit meter
$(S'_{gen})_F$	[W/m]	Entropy generation per unit meter due to fluid flow
$(S'_{gen})_H$	[W/m]	Entropy generation per unit meter due to heat transfer
T	[K]	Temperature
V	[m/s]	Velocity
$\dot{V}$	[m^3/s]	Volumetric flow rate
x	[m]	Cartesian axis direction
y	[m]	Cartesian axis direction

Greek symbols

α	[-]	Absorptivity
β	[K^{-1}]	Coefficient of thermal expansion
ρ	[-]	Collector reflectance
φ_r	[degrees]	Collector rim angle
σ	[W/m^2K^4]	Stefan Boltzmann constant
θ	[degrees]	Receiver circumferential angle
ε	[-]	Emissivity
τ_g	[-]	Glass cover transmissivity
ν	[Pa s]	Kinematic viscosity

Subscripts

amb	Ambient state
air	Air
air,o	Air at standard temperature and pressure
eff	Effective value
gi	Glass cover inner wall
go	Glass cover outer wall
Inlet	Inlet
L	Characteristic length
opt	Optimum operating condition
ri	Absorber tube inner wall
ro	Absorber tube outer wall
Sky	Sky temperature
w	Wind

Several studies to characterise the performance of the parabolic trough receiver have been reported in literature. These studies include steady state tests in the laboratory, actual field tests as well as numerical investigations. In steady-state laboratory tests, the receiver is supplied with an electrical current to raise its temperature to a certain value. The amount of power input required to keep this temperature is the receiver's heat loss [2-5]. In this method, the non-uniformity of the heat flux on the receiver's absorber tube is not accounted for. Experiments under actual operating conditions provide a comprehensive means of characterising the performance of the entire collector at a given point in time [6-8] . Even though, this is the best approach the costs of such experiments especially for different combinations of geometrical parameters may be prohibitive. With the advances in computing and computing power, use of numerical methods has been widely adopted in engineering design. Regarding parabolic trough systems, several numerical investigations are available in literature [9-15]. Some of these numerical investigations use the simplified heat flux profile while others use actual non-uniform heat flux on the absorber tube.

Increasing concentrator sizes is one of the ways to reduce further the cost of electricity generated from parabolic trough systems [16]. With the availability of lightweight materials, the use of large concentration ratios has become possible. This reduces the number of collectors used, thus reducing the number of drives and controls. As concentration ratios increase, the thermal and thermodynamic performance of the receiver will be affected. In our earlier investigation [15], increasing the concentration ratio was shown to increase the entropy generation rates in the parabolic receiver. This was due to increasing heat transfer irreversibility due to a higher finite temperature difference as the concentration ratios increased. In that study, the effect of a combination of rim angles and concentration ratios was not investigated. Moreover, most studies on thermal performance of parabolic trough receivers do not account for the effect of collector geometry on the thermal and thermodynamic performance. Other studies found in literature use simplified profiles for heat flux on the receiver's absorber tube. In this paper, we focus on the characterisation of the thermal and thermodynamic performance of the parabolic trough receiver at different combinations of rim angles and concentration ratios using actual non-uniform heat flux profiles.

PHYSICAL MODEL

Figure 1(a) shows the 3-D model of a parabolic trough collector under consideration. Figure 1(b) shows the cross-section view of the receiver. Figure 2 shows the cross-section view of the parabolic trough collector together with the receiver's absorber tube and a trace of some of the incident rays. The most important geometrical parameters considered in the design of a parabolic trough collector are the rim angle (φ_r), the focal length (f) and the aperture width (a) as shown in Figure 2. The geometry of the collector is defined by

$$y^2 = 4fx \tag{1}$$

The focal length is related to the rim angle and aperture width as

$$f = a/4\tan(\varphi_r/2) \tag{2}$$

From equation (2), given any two parameters, the third parameter can be calculated. Usually, the aperture and the rim angle are specified and the focal length or the ratio (f/a) can be obtained. The concentration ratio used in this study relates the projected area of the collector to the projected area of the absorber tube as $C_R = A_a/A_r$. The other equations that define the geometry of the collector, receiver and the minimum size required to intercept the sun's image are given in Duffie and Beckman [17]. Similar to conventional receivers, the receiver's annulus space is considered evacuated to very low pressures (about 0.013 Pa)[18]. The receiver's absorber tube has an outer wall that is coated with a cermet selective coating.

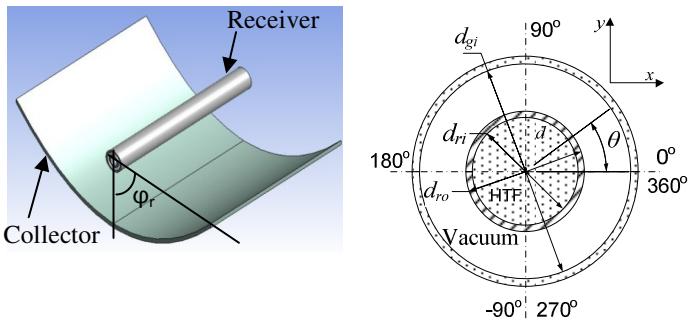

(a) (b)

Figure 1 (a) 3-D model of parabolic trough collector (b) cross-section view of the receiver

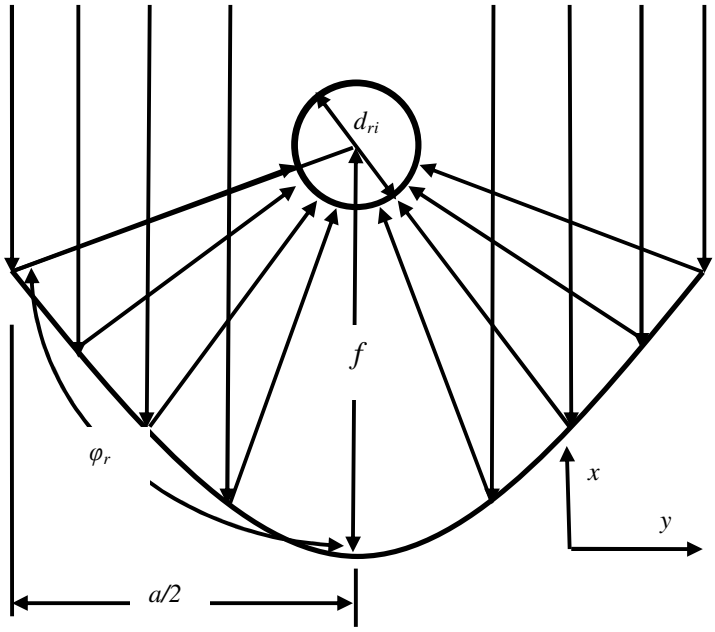

Figure 2 Collector cross-section view

In Figure 2, a is the aperture width, d_{ri} is the absorber tube diameter, φ_r is the rim angle and f is the focal length.

The receiver's thermal loss generally depends on whether the absorber tube is enclosed by a glass cover. If enclosed, on whether the annulus space is evacuated or not. For a receiver with an evacuated glass envelope such as the ones used in conventional parabolic trough plants, the receiver thermal loss is [17]

$$Q_{loss} = \frac{2\pi k_{eff,air} L}{\ln \frac{d_{gi}}{d_{ro}}}\left(T_{ro} - T_{gi}\right) + \frac{\pi d_{ro} L \sigma \left(T_{ro}^{\ 4} - T_{gi}^{\ 4}\right)}{\frac{1}{\varepsilon_{ro}} + \frac{1-\varepsilon_{gi}}{\varepsilon_{gi}}\left(\frac{d_{ro}}{d_{gi}}\right)} \quad (3)$$

Equation (3), gives the thermal loss from the absorber tube to the glass cover.

An energy balance easily shows that the thermal loss in equation (3) is equivalent to the heat loss from the glass cover to the surroundings according to

$$Q_{loss} = \pi d_{go} L h_w (T_{go} - T_{amb}) + \varepsilon_{go} \pi d_{go} L \sigma \left(T_{go}^{\ 4} - T_{sky}^{\ 4}\right) \quad (4)$$

In equation (3), $k_{eff,air}$ is the effective thermal conductivity of air between the glass cover and the absorber tube given by equation (5) quoted in Duffie and Beckman [17].

$$\frac{k_{eff,air}}{k} = \max\left[1,\quad 0.386\left(\frac{\Pr x Ra^*}{0.861+\Pr}\right)^{\frac{1}{4}}\right] \quad (5)$$

Where

$$Ra^* = \frac{\left(\ln d_{ro}/d_{ri}\right)^4}{L^3\left(d_{ri}^{-3/5} + d_{ro}^{-3/5}\right)^5} Ra_L \quad (6)$$

And

$$Ra_L = \frac{g\beta(T_{ro} - T_{gi})L^3 \Pr}{v^2} \quad (7)$$

In equation (6) and equation (7) L is the characteristic length. In this case, the spacing between the absorber tube and the glass cover.

For very low vacuum pressures $k_{eff,air}$ approaches zero and only radiation heat transfer in equation (3) is considered. Air thermal conductivity for low pressures is given by equation (8) [19]

$$k_{air} = k_{air,o} \frac{1}{1 + \frac{7.6x10^{-5}}{P\, d_c/T}} \quad (8)$$

In which, d_c is the spacing between the glass cover and the absorber tube.

The sky temperature is related to the ambient temperature as [20]

$$T_{sky} = 0.0552 T_{amb}^{1.5} \quad (9)$$

The emissivity of the glass is given as ε_{gi} = 0.86 [21] whereas the absorber tube emissivity varies with wall temperature. For an absorber tube with a cermet selective coating, the emissivity is given by [21]

$$\varepsilon_{ro} = 0.000327(T_{ro} + 273.15) - 0.065971 \quad (10)$$

The average wind heat transfer coefficient on the receiver's glass cover was determined using the expression given by [22] as

$$h_w = V_w^{0.58} d_{go}^{-0.42} \quad (11)$$

In which, V_w is the wind speed.

NUMERICAL METHOD

Boundary Conditions

The boundary conditions used in this study were: (1) Non-uniform heat flux on the absorber tube's outer wall. The sample heat flux distribution used in this study is shown in Figure 3 as determined using ray tracing in SolTrace [23] for rim angles of 80° and 120° and an aperture width of 6 m or concentration ratio(C_R) of 86. A direct normal irradiance (DNI) of 1000 W/m^2 was assumed throughout this work. The collector is assumed to be of perfect alignment and perfect shape. (2) Velocity inlet and pressure outlet boundary conditions were used for the absorber tube's inlet and outlet respectively. (3) No-slip and no-penetration boundary condition was specified for the inner absorber tube wall. (4) For the inlet and outlet of the receiver's

annulus space, a symmetry boundary condition was used such that the normal gradients of all flow variables are zero. (5) On the outer wall of the glass cover, a mixed boundary condition is used to account for both radiation and convection heat transfer. Stefan Boltzmann's law gives radiation between the glass cover and the sky. The sky is taken as a large enclosure. Convection heat transfer from the receiver's glass was modelled by specifying a convection heat transfer coefficient and free stream temperature. The sky temperature is given by equation (9) while the wind heat transfer coefficient is given by equation (11). The ambient temperature was kept at 300 K and the wind speed was fixed at 2 m/s. Table 1, shows the summary of the other parameters used in this study.

Table 1. Geometrical and optical values of the parabolic trough collector

Parameter	Value	Parameter	Value
a	4 - 10 m	d_{ri}	0.066 m
L	5.0 m	d_{ro}	0.07 m
ρ	0.96	τ_g	0.97
φ_r	40-120^o	α	0.96
$C_R=A_c/A_r$	57.12-142.86		

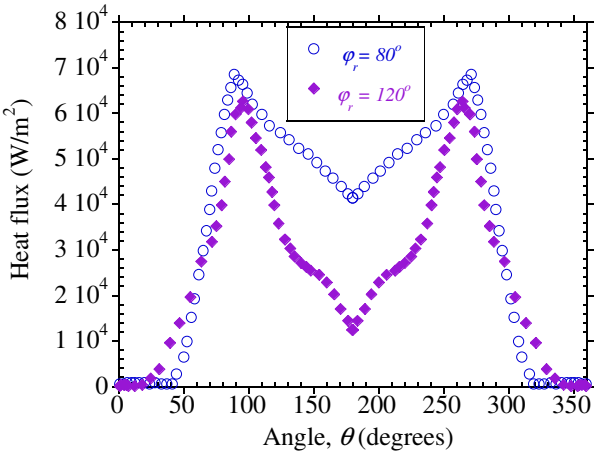

Figure 3 Sample heat flux distribution on the entire circumference of the absorber tube

Computation Procedure

In this study, a computational fluid dynamics tool was used to study the thermal and thermodynamic performance of the receiver. The procedure involved solution of the Reynolds averaged Navier-Stokes equations using the finite volume method implemented in a commercial computational fluid dynamics code, ANSYS Fluent [24]. The computational domain was discretised using hexahedral and quadrilateral elements. Second order upwind scheme ware employed for integrating the governing equations together with the boundary conditions over the computational domain. The SIMPLE algorithm was used for coupling pressure and velocity. Radiation heat transfer in the annulus was modelled using the discrete ordinates model. In order to capture the near wall gradients, the dimensionless wall coordinate y^+ of about 1 was ensured in all simulations. The realisable k- ε model [25] was used for turbulence modelling. The enhanced wall treatment option was used for modelling the near-wall regions. Convergence was obtained with scaled residuals of mass, momentum, turbulent kinetic energy (k) and turbulence dissipation rate (ε) less than 10^{-4} while the energy residuals were less than 10^{-6}. Solution was taken to be fully converged when the convergence history of the absorber outlet temperature, glass temperature and entropy generation flattened for more than 200 successive iterations.

The heat transfer fluid used is syltherm800 and its properties are temperature dependent as determined from the manufacturer's data sheets. The polynomials used are given in a previous investigation [15].

Validation of Numerical Models

Our numerical results have been validated with data available in literature. The validation of the ray trace results is shown in Figure 4. The same trend exists when compared to the results of Jeter [26], He *et al.* [9] and Yang *et al.* [27]. Good agreement was obtained in comparison with data from He *et al.* [9] and Yang *et al.* [27] for the entire range of receiver circumferential angle. LCR is the local concentration ratio, which is the ratio of the actual heat flux on the absorber tube to the incident solar radiation.

The validation of the thermal performance of the receiver model was done using data from Sandia national laboratories. In the validation of the receiver thermal model, a collector module with an aperture of 5 m, a length of 7.8 m, focal length of 1.49 and geometrical concentration ratio of 71 was used with similar parameters as was used in the experiment [6]. At each inlet temperature shown in Figure 5, the experimental conditions are different as shown in Table D-1 presented in the test results of Dudley *et al.* [6] for a Cermet coated receiver. Good agreement was achieved for heat transfer fluid temperature gain and collector efficiency except for the 3rd last point where the experimental results indicated a higher efficiency. High deviations are shown to exist at higher fluid temperatures. This is probably because the heat loss to the receiver supports is significant as the temperatures increase. This was considered negligible in our modelling.

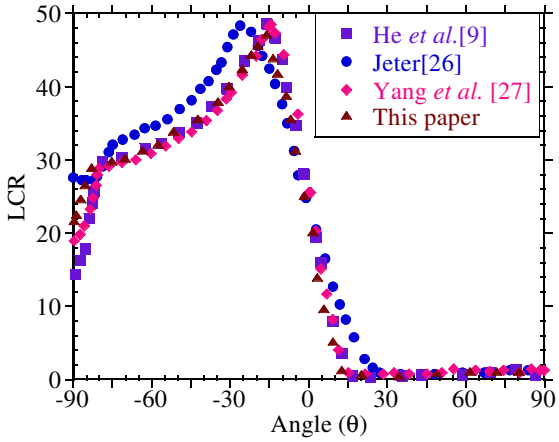

Figure 4 Validation of ray trace results

For thermodynamic characterisation, the entropy generation due to heat transfer and fluid flow irreversibilities was obtained numerically using the method and equations suggested by Kock and Herwig [28,29]. The method involves determination of the entropy generation due to heat transfer and fluid flow in the post processing stage of the computational fluid dynamics analysis. In this study, these equations are written as custom field functions. The validation of the entropy generation model and the relevant equations were presented in our earlier work [15] and will not be presented again.

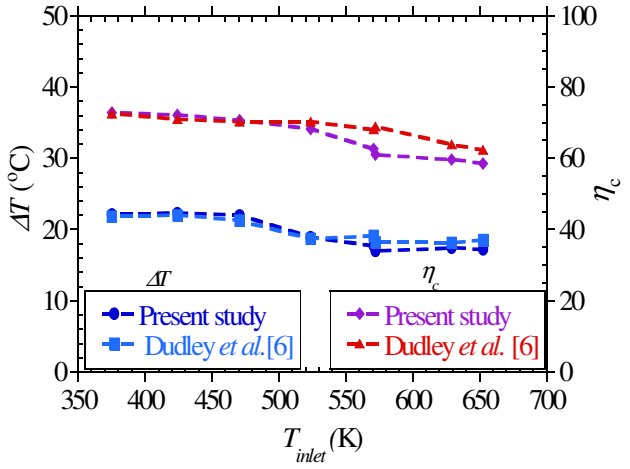

Figure 5 Validation of the receiver model

RESULTS AND DISCUSIONS

Figure 6 shows the heat flux profiles at different values of rim angles. As shown, the heat flux distribution on the receiver's absorber tube is not uniform. It is characterised by an area where collector shadows the tube depending on the rim angle (at a rim angle of 120°, this area is in the range $-90^{o} \leq \theta \leq -80^{o}$). An area where the heat flux is increasing also depending on the rim angle (is in the range $-80^{o} \leq \theta \leq 15^{o}$, at a rim angle of 120°). An area where the heat flux is reducing, also depending on the rim angle (is in the range $15^{o} \leq \theta \leq 55^{o}$, at a rim angle of 120°). And an area where only direct solar radiation is incident on the absorber tube (in the range $55^{o} \leq \theta \leq 90$ at a rim angle of 120°).

These regions are more distinct at rim angles above 60°. The shadow effect is significant as the rim angles increase, while the area receiving direct solar radiation reduces as the rim angles increase. The figure also shows that the peak heat flux increases as the rim angle reduces. At rim angles above 80°, the change in the peak heat flux is not significant. At a rim angle of 40°, there is almost no shadowing effect and no heat flux increasing area. The heat flux will be concentrated on the half of the absorber tube facing the collector. As shown, at such low rim angles, high heat flux peaks will result and large temperature gradients will result.

Figure 7 shows the variation heat flux with concentration ratio, as expected increasing the concentration ratio increases the heat flux on the receiver.

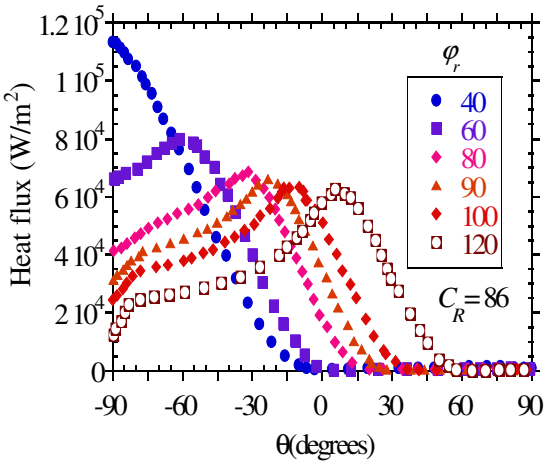

Figure 6 Variation of heat flux with rim angle

This heat flux distribution on the receiver results in non-uniform temperature distribution on the receiver's absorber tube as shown in Figure 8. This results in temperature gradients in the receiver, which might lead to failure of the glass cover due to the induced stresses.

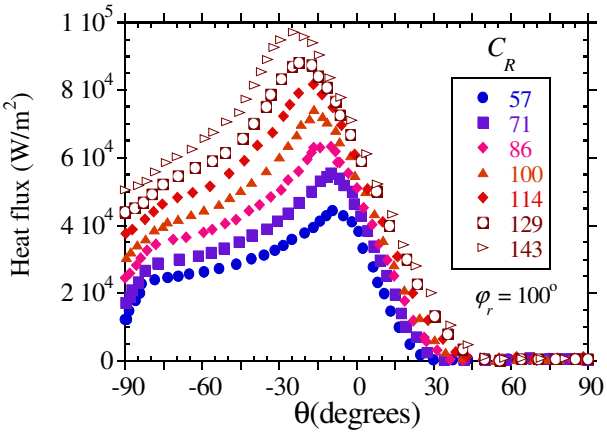

Figure 7 Variation of heat flux with receiver angle at different concentration ratios

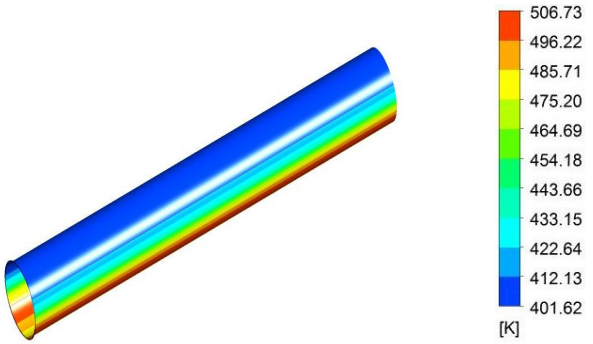

Figure 8 Temperature contours on the absorber tube at Re = 11,050, T_{inlet} = 400 K, φ_r = 80°, C_R = 85.70

An important factor to consider in the analysis of the parabolic trough systems is the absorber tube temperature gradients. The maximum temperature difference for safe operation is about 50°C. As shown in Figure 9 and Figure 10, the absorber tube temperature difference increases as rim angle reduces and as the concentration ratio increases respectively.

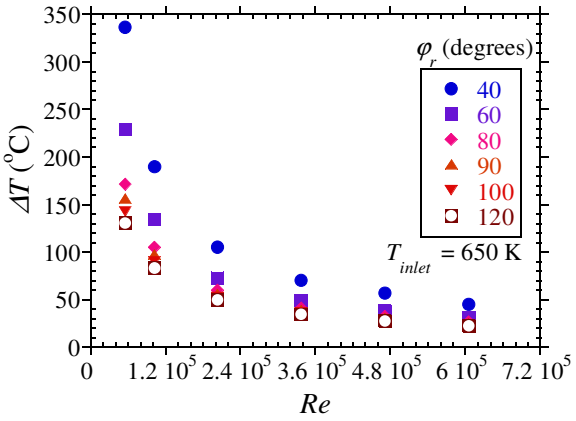

Figure 9 Variation of absorber tube temperature gradient with Reynolds number at different rim angles

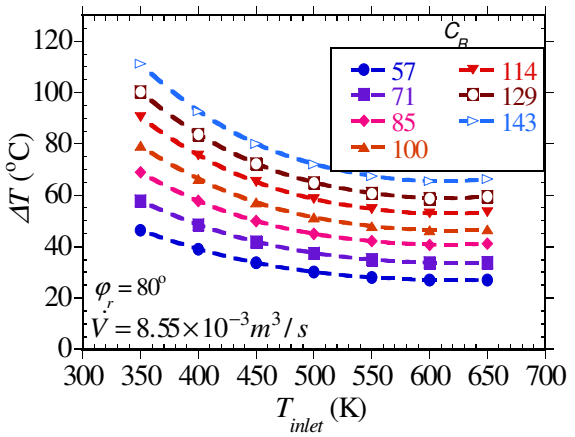

Figure 10 Variation of absorber tube temperature gradient with inlet temperature at different concentration ratios.

At a flow rate of 8.55 × 10^{-3} m^3/s (flow rates in commercial plants [21]) the temperature gradients are within less than 50°C at all fluid temperatures and rim angles except when the concentration ratios increase above 100.

Figure 11 shows the variation of receiver thermal loss with inlet temperature. Generally, the thermal loss increases as the inlet temperature increases. At high inlet temperatures, the absorber tube temperatures are high and thus the radiation heat loss is high. The radiation heat loss increases further because, the emissivity of the absorber tube increases with absorber tube temperature.

Figure 11 also shows that, the thermal loss increases slightly as the rim angle reduces. As earlier discussed, low rim angles lead to higher heat flux peaks and thus higher temperature peaks. The variation of receiver thermal loss with rim angle becomes negligible at higher flow rates due to better heat transfer and significant reduction in temperature gradients.

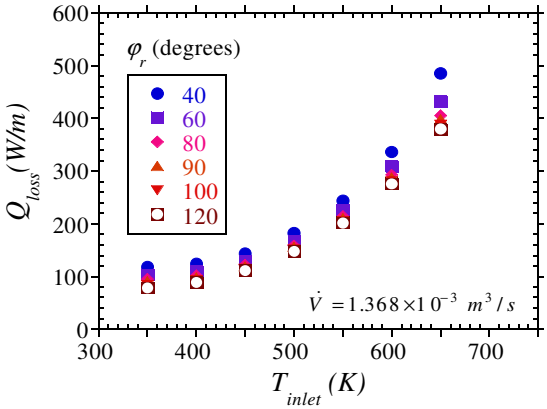

Figure 11 Variation of receiver thermal loss with inlet temperature at different rim angles

In Figure 12, the variation of receiver thermal loss with inlet temperature at different concentration ratios is presented. As seen in the figure, the general trend of increasing thermal loss with inlet temperature exists [3]. At very low flow rates, the increase in thermal loss as the concentration increases is very significant.

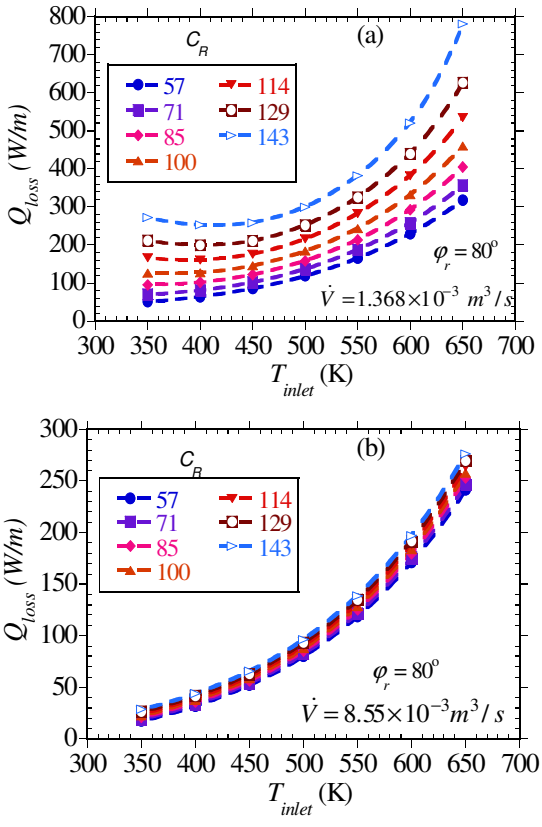

Figure 12 Variation of receiver thermal loss with inlet temperature at different concentration ratios (a) at 1.368×10^{-3} m^3/s (b) 8.55×10^{-3} m^3/s.

For example, at a flow rate of 1.368×10^{-3} m^3/s, the thermal loss increases from 229 W/m at a concentration ratio of 57 to 520 W/m at a concentration ratio of 143 when the rim angle is 80^o and inlet temperature is 600 K as shown in Figure 12 (a).

At a flow rate of 8.55×10^{-3} m^3/s, close to the maximum flow rates in commercial plants, the thermal loss increases from about 170 W/m at a concentration ratio of 57 to 196 W/m at a concentration ratio of 143 for a rim angle of 80^o and inlet temperature of 600 K as shown in Figure 12(b). At the flow rates in current commercial plants, the thermal loss increases only slightly as the concentration ratio increases. The increase in the thermal loss as the concentration ratio increases can be attributed to higher absorber tube temperatures from high heat fluxes as the concentration ratios increase. At high flow rates, the heat transfer rates are higher and increasing the concentration ratio does not significantly affect the receiver thermal performance.

To characterise the thermodynamic performance of engineering systems, the determination of the entropy generation rates is essential to show which system configuration give the lowest entropy generation rates. This method, initially suggested by Bejan [30] has grown and become a useful tool for thermodynamic design and optimisation of thermal systems. In this study, the heat transfer and fluid flow irreversibilities in the receiver's absorber tube were determined from which the total entropy generation rates was obtained.

Generally, the fluid flow irreversibility will increase as the Reynolds numbers increase due to increase pressure drop while the heat transfer irreversibility will reduce as the Reynolds number increase due to reduced finite temperature differences as shown in Figure 13. From this variation, the entropy generation is a minimum at a Reynolds number referred to as an optimal Reynolds number. Figure 14 shows the variation of the entropy generation rate in the receiver due to heat transfer and fluid flow with Reynolds number at different rim angles.

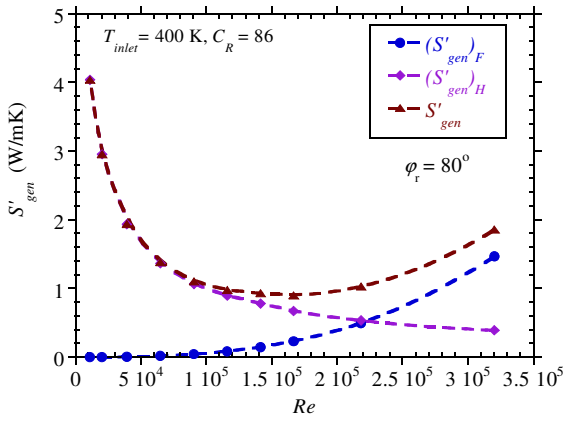

Figure 13 Variation of entropy generation with Reynolds number

Similar to Figure 13, there is an optimal Reynolds number gives minimum entropy generation. As shown, smaller rim angles give higher values of entropy generation compared to larger angles. This is because, at lower rim angles, the peak temperatures in the receiver are higher and thus lead to higher heat transfer irreversibilities. As the rim angles increases to over 80^o, the entropy generation rates do not change significantly given that at these angles, the change in the peak heat flux as the angle increase is not significant as earlier discussed.

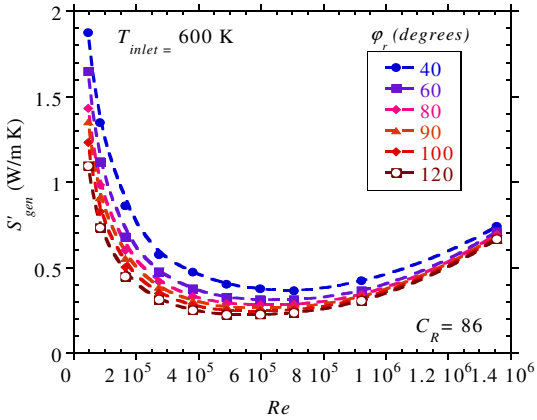

Figure 14 Variation of entropy generation with Reynolds number at different rim angles

Figure 15 shows the variation of entropy generation with concentration ratio. Generally, increasing concentration ratios increase the heat flux on the absorber tube and as such increases the finite temperature difference and the heat transfer irreversibility. As discussed in our previous investigation [15], the entropy generation rates will reduce as the fluid temperatures reduce.

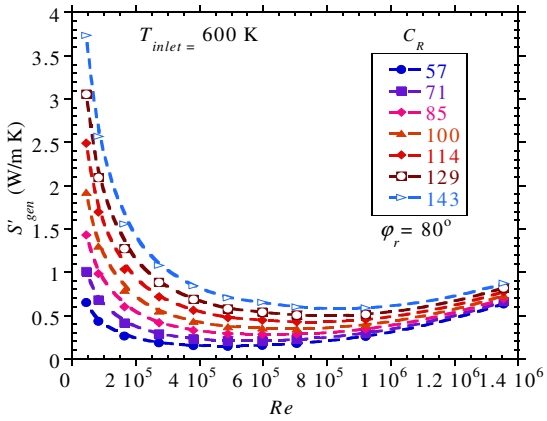

Figure 15 Variation of entropy generation with Reynolds number at different concentration ratios

As earlier discussed, the entropy generation is a function of both the heat transfer and fluid friction irreversibility. To show the relative contribution of each irreversibility to the total entropy generation rate, the Bejan number, *Be* is used. The Bejan number is the ratio of the heat transfer irreversibility to the total entropy generation rate. As shown in Figure 16 and 17, the Bejan number increases as the rim angle reduces and as the concentration ratio increases. This shows that, the increase in entropy generation as rim angles reduce and as the

concentration ratios increase is mainly due to increase in heat transfer irreversibility.

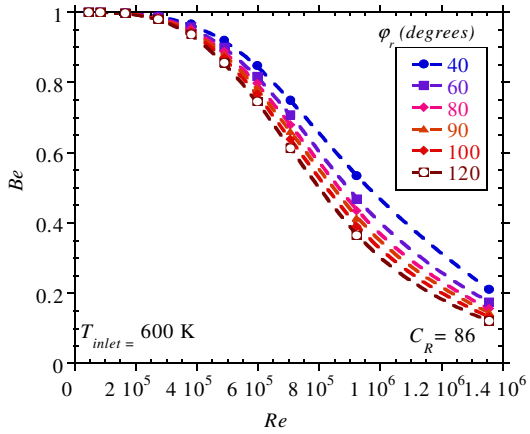

Figure 16 Variation of Bejan number with Reynolds number at different rim angles

The figures also show the Bejan number to reduce as the Reynolds numbers increase, this is mainly due to improved heat transfer and reduction of heat transfer irreversibilities accompanied with increasing fluid friction irreversibilities.

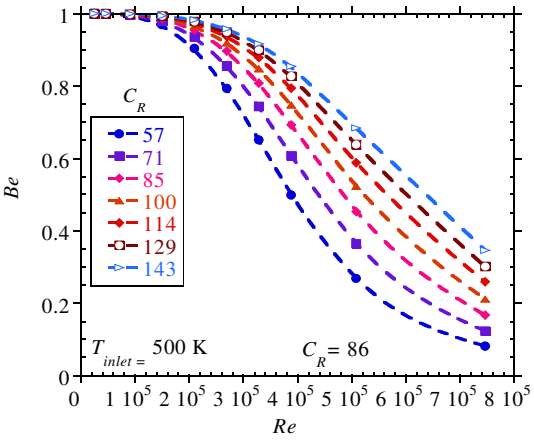

Figure 17 Variation of Bejan number with Reynolds number at different concentration ratios

At every rim angle and concentration ratio, the optimal Bejan number and optimal Reynolds number can be obtained at the optimal operation points in figures 14 and 15, i.e. points with minimum entropy generation. Figure 18 shows the variation of the optimal Bejan number and optimal Reynolds number with rim angle at different inlet temperatures at a concentration ratio of 86. Generally, at a given concentration ratio, the optimal Bejan number reduces as the rim angle increases; this is because an increase in rim angles reduces the peak heat flux on the absorber tube thus reducing the heat transfer irreversibility. The optimal Reynolds number is shown to remain constant as the rim angle increases at any given temperature. Even though, the Reynolds number increases as the temperatures increase, the flow rate is the same for all inlet temperatures at a given concentration ratio. At a concentration ratio of 86 shown in figure 18, the optimal flow rate is 0.0222 m^3/s.

The variation of optimal Bejan number and optimal Reynolds number with concentration ratio is show in Figure 19. As shown, the optimal Bejan number decreases as the concentration ratio increases. The optimal Reynolds slightly increases as the concentration ratio increases. As the concentration ratios increase, heat transfer irreversibilities increase and as such higher flow rates are required to reduce these irreversibilities. This leads to a decrease in optimal Bejan number and an increase in the optimal Reynolds number.

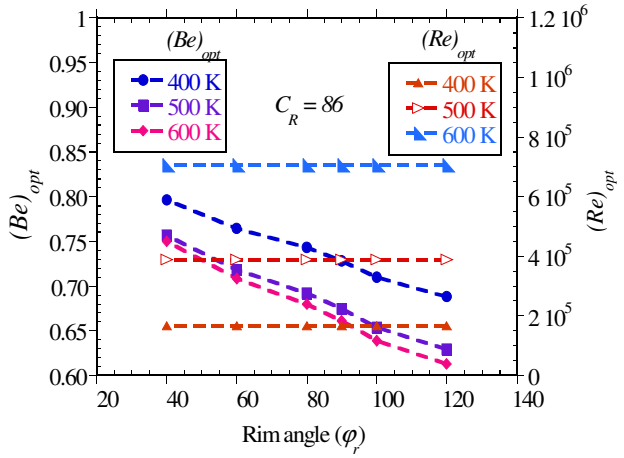

Figure 18 Variation of optimal Bejan number and optimal Reynolds number with rim angle at different inlet temperatures

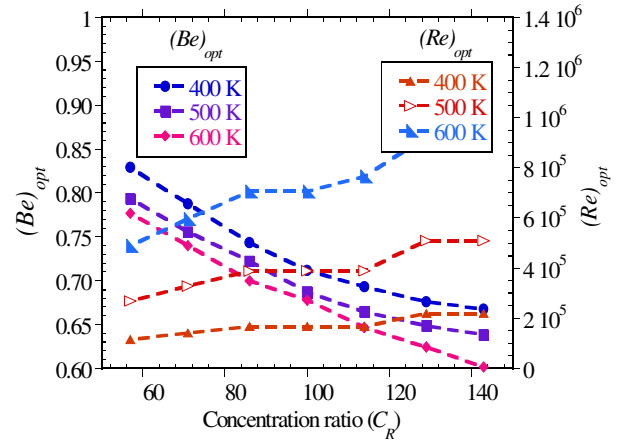

Figure 19 Variation of optimal Bejan number and optimal Reynolds number with concentration at different inlet temperatures

CONCLUSION

In this paper, the thermal and thermodynamic performance of a parabolic trough receiver at different concentration ratios and rim angles was discussed. The influence of a combination of rim angles, Reynolds numbers and concentration ratio on the heat flux and temperature distribution in the receiver was presented and discussed. Moreover, the influence of different

rim angles and concentration ratio on entropy generation rates was also presented.

The heat flux and temperature distribution are shown to be non-uniform along the absorber tube's circumference. From the study, the use of low rim angles and high concentration ratios is shown to increase temperature gradients in the receiver. These temperature gradients are very high at low Reynolds numbers. The influence of rim angles on the receiver's thermal performance was shown to be insignificant at flow rates close or than 8.55×10^{-3} m^3/s.

From the thermodynamic analysis, the use of low rim angles and high concentration ratios increases the entropy generation rates in the receiver. This is attributed to the increase in the finite temperature difference in the receiver as the concentration ratio increases. The presence of an optimal Reynolds number at each value of concentration ratio at a given rim angle was demonstrated.

In general, at rim angles greater than 80^o, the increase in absorber tube temperature gradients and entropy generation is shown to be insignificant. However, as the concentration ratios increase, the temperature gradients as well as entropy generation in the receiver continues to increase. Thus careful matching of the flow rates with incident solar radiation is essential to keep the temperature gradients at desirable levels at every chosen concentration ratio.

REFERENCES

[1] Kalogirou S., Solar energy engineering: processes and systems. 1st ed. Oxford, UK: Elsevier, Academic Press, 2009.

[2] Lüpfert E., Riffelmann K., Price H., Burkholder F, and Moss T., Experimental analysis of overall thermal properties of parabolic trough receivers, *Journal of Solar Energy Engineering,* Vol. 130, 2008, 021007.

[3] Burkholder F., and Kutscher C., Heat loss testing of Schott's 2008 PTR70 parabolic trough receiver, National Renewable Energy Laboratory, REL/TP - 550-45633, 2009, pp. 1-58.

[4] Burkholder F., and Kutscher C., Heat-loss testing of Solel's UVAC3 parabolic trough receiver, National Renewable Energy Laboratory, NREL/TP - 550-42394, 2008, pp. 1-19.

[5] Lei D., Li Q., Wang Z., Li J., and Li J., An experimental study of thermal characterization of parabolic trough receivers, *Journal of Energy Conversion and Management*, Vol. 69, 2013, pp. 107-115.

[6] Dudley E.V., Kolb J.G., Mahoney A.R., Mancini T.R., Sloan M., and Kearney D., Test results: SEGS LS-2 solar collector. Sandia National Laboratory, SAND94-1884,1994.

[7] Dudley E.V., Evans R.L., Mathews W.C., Test results: Industrial Solar Technology parabolic trough solar collector, Sandia National Laboratory, SAND94-1117, 1995.

[8] Liu Q.B., Wang Y.L., Gao Z.C., Sui J., Jin H.G., and Li H.P., Experimental investigation on a parabolic trough solar collector for thermal power generation. *Science China Series E-Technological Science*, Vol. 53, 2010, pp. 52-56.

[9] He Y., Xiao J., Cheng Z., and Tao Y., A MCRT and FVM coupled simulation method for energy conversion process in parabolic trough solar collector, *Journal of Renew Energy*, Vol. 36, 2011, pp. 976-985.

[10] Gong G., Huang X., Wang J., and Hao M., An optimized model and test of the China's first high temperature parabolic trough solar receiver, *Journal of Solar Energy,* Vol. 84, 2010, pp. 2230-2245.

[11] Muñoz J., and Abánades A., Analysis of internal helically finned tubes for parabolic trough design by CFD tools, Journal of Applied Energy, Vol. 88, 2011, pp. 4139-4149.

[12] Naeeni N., and Yaghoubi M., Analysis of wind flow around a parabolic collector (2) heat transfer from receiver tube, *Journal of Renewable Energy,* Vol. 32, 2007, pp. 1259-1272.

[13] Roesle M., Coskun V., and Steinfeld A., Numerical analysis of heat loss from a parabolic trough absorber tube with active vacuum system, *Journal of Solar Energy Engineering*, Vol. 133, 2011, pp. 031015-1 - 031015-5.

[14] Ravi Kumar K., and Reddy K.S., Numerical investigation of energy-efficient receiver for solar parabolic trough concentrator, J*ournal of Heat Transfer Engineering,* Vol.29, 2008, pp. 961-972.

[15] Mwesigye A., Bello-Ochende T., and Meyer J.P., Numerical investigation of entropy generation in a parabolic trough receiver at different concentration ratios, *Journal of Energy,* Vol. 53, 2013, pp. 114-127.

[16] SunShot Initiative, available at: http://www1.eere.energy.gov/solar/sunshot/index.html, Last accessed [12/02/2013] .

[17] Duffie J.A., and Beckman W.A., Solar engineering of thermal processes, 3rd ed. Hoboken, New Jersey: *John Wiley and Sons Inc*., 2006.

[18] Price H., Lüpfert E., Kearney D., Zarza E., Cohen G., Gee R., and Mahoney R., Advances in parabolic trough solar power technology. *Journal of Solar Energy Engineering,* Vol. 124, 2002, pp. 109-25.

[19] Potkay A.J., and Sacks D.R., A low-power pressure-and temperature-programmable micro gas chromatography column, *Journal of Microelectromechanical Systems*, Vol. 16, 2007, pp. 1071-1079.

[20] García-Valladares O., and Velázquez N., Numerical simulation of parabolic trough solar collector: Improvement using counter flow concentric circular heat exchangers. *International Journal of Heat and Mass Transfer*, Vol. 52, 2009, pp. 597-609.

[21] Forristall R., Heat transfer analysis and modeling of a parabolic trough solar receiver implemented in Engineering Equation solver. *NREL Technical Report,* NREL/TP-550-34169, October 2013, pp. 1-145.

[22] Mullick S.C., and Nanda S.K., An improved technique for computing the heat loss factor of a tubular absorber, *Journal of Solar Energy,* Vol. 42, 1989, pp. 1-7.

[23] SolTrace optical modelling software, SolTrace v.2012.7.9, available at: http://www.nrel.gov/csp/soltrace/, Last accessed [12/02/2013]

[24] ANSYS® Academic research, release 14.5, ANSYS FLUENT user's guide, ANSYS, Inc.

[25] ANSYS® Academic research, release 14.5, ANSYS FLUENT, theory guide, ANSYS, Inc.

[26] Jeter S.M., Calculation of the concentrated flux density distribution in parabolic trough collectors by a semifinite formulation, *Journal of Solar Energy,* Vol. 37, 1986, pp. 335-345.

[27] Yang B., Zhao J., Xu T., and Zhu Q., Calculation of the concentrated flux density distribution in parabolic trough solar concentrators by Monte Carlo ray-trace method, *Journal of Photonics and Optoelectronic (SOPO)*, 2010, pp. 1-4.

[28] Herwig H., and Kock F., Direct and indirect methods of calculating entropy generation rates in turbulent convective heat transfer problems, *Journal of Heat and Mass Transfer*, Vol. 43, 2007, pp. 207-215.

[29] Kock F., and Herwig H., Local entropy production in turbulent shear flows: a high-Reynolds number model with wall functions, *International Journal of Heat and Mass Transfer,* Vol. 47, pp. 2205-2215.

[30] Bejan A., A study of entropy generation in fundamental convective heat transfer, *Journal of Heat Transfer*, Vol. 101, 1979, pp. 718-725.